Quantum Chaos with Cold Cesium Atoms

W. H. Oskay, D. A. Steck, B. G. Klappauf, and M. G. Raizen

Department of Physics, The University of Texas at Austin, Austin, Texas, 78712-1081 USA
e-mail: raizen@physics.utexas.edu
Received August 27, 1998

Abstract—Atomic motion in a time-dependent standing wave of light provides an almost ideal experimental system for the study of quantum chaos, due to the nonlinearity of the potential combined with negligible dissipation. In our first experiments with sodium atoms we observed dynamical localization, a quantum suppression of chaotic diffusion. To go beyond this work we have constructed an experiment with cold cesium atoms, and report our first results from this system. The larger mass and longer wavelength push out the momentum boundary in phase space that arises from the nonzero duration of the pulses. This feature should enable the study of effects leading to delocalization.

1. INTRODUCTION

The meeting ground between quantum mechanics and nonlinear dynamics has developed into a new field of research known as quantum chaos. One of the key predictions in this field is dynamical localization. This striking effect is a quantum suppression of classical (chaotic) diffusion, and has stimulated a great deal of interest and discussion since it was first predicted almost twenty years ago [1–7].

Quantum mechanics and nonlinear dynamics come together naturally in atom optics with laser cooled atoms. The nonlinear potential, created by a standing wave of light, can be modulated to produce a system that is classically chaotic. Since dissipation can be made negligibly small in this system, quantum effects can become important. These features led to a series of experiments in our group on dynamical localization and quantum chaos with cold sodium atoms, establishing atom optics as a new experimental testing ground for the field [8–12]. The simplest experimental configuration in that work was a standing wave of light that was pulsed on periodically. This system was an experimental realization of the kicked rotor, which has been a paradigm for classical and quantum chaos for many years.

To go beyond this first generation of experiments, we have built a new experiment based on laser cooled and trapped cesium. This paper describes our first experiments in this new system, which is a realization of the quantum kicked rotor, and presents a study of boundary effects on dynamical localization. In Section 2 we give a theoretical background on atomic motion in a far-detuned dipole potential, and provide a classical analysis of the boundary in phase space. In Section 3 we describe the general experimental approach. In Section 4 we discuss the new experimental results with cesium. Finally, in Section 5 we describe some directions for future work.

2. THEORETICAL BACKGROUND

To describe our system we begin with a two-level atom with transition frequency ω_0 interacting with a pulsed standing wave of linearly polarized, near-resonant light of frequency ω_L. For sufficiently large detuning $\delta_L = \omega_0 - \omega_L$ (relative to the natural linewidth), the excited state amplitude can be adiabatically eliminated [13]. The atom can then be treated as a point particle. This approximation leads to the following kicked-rotor Hamiltonian for the center-of-mass motion of the atom:

$$H = \frac{p^2}{2M} + V_0 \cos(2k_L x) \sum_{n=-\infty}^{\infty} F(t - nT). \qquad (1)$$

Here $V_0 = \hbar\Omega^2/8\delta_L$, k_L is the wave number of the light, $\Omega = 2\mu E_0/\hbar$ is the resonant Rabi frequency, μ is the atomic dipole moment, E_0 is the electric field of a single travelling wave component of the standing wave, $F(t)$ is a pulse centered at $t = 0$ with duration t_p, and T is the period of the standing wave pulses. It is convenient to rescale our coordinates and use the dimensionless Hamiltonian

$$H = \rho^2/2 + k\cos(\phi) \sum_{n=-\infty}^{\infty} f(\tau - n), \qquad (2)$$

where $\phi = 2k_L x$, $\rho = (2k_L T/M)p$, $\tau = t/T$, $f(\tau)$ is a pulse of unit amplitude and scaled duration $\alpha = t_p/T$, $k = (8V_0/\hbar)\omega_r T^2$ is the scaled kick amplitude, $\omega_r = \hbar k_L^2/2M$ is the recoil frequency, $H' = (4k_L^2 T^2/M)H$, and we have dropped the prime on H. In the quantized model, ϕ and ρ are conjugate variables that satisfy the commutation relation $[\phi, \rho] = i\bar{k}$, where $\bar{k} = 8\omega_r T$ is a scaled Planck constant. In the limit where $f(\tau)$ becomes a δ-function, the product ηk reduces to the classical stochasticity parameter K for the δ-kicked rotor, where $\eta = \int_{-\infty}^{\infty} f(\tau)d\tau$. The stochasticity parameter completely

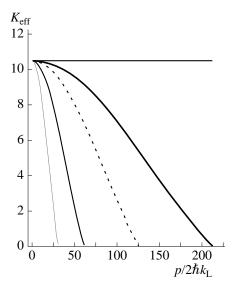**Fig. 1.** Classical calculation of the effective stochasticity parameter K_{eff} as a function of momentum for square pulses of various temporal widths. The horizontal line represents the δ-kick case. The other curves represent square pulses with widths $\alpha = 0.014$ (heavy solid line), $\alpha = 0.024$ (dashed), $\alpha = 0.049$ (dash-dot), and $\alpha = 0.099$ (dotted). The well depth is adjusted in each case to give the same maximum value of $K_{eff} = 10.5$ at $\alpha = 0$. The point where K_{eff} drops to ~1 in each case is the classical momentum boundary. The typical limit of our momentum measurements is $|p/2\hbar k_L| \approx 80$. Note that we have suppressed the curves after their first zero-crossing.

specifies the classical δ-kicked rotor dynamics. For $K \gtrsim 1$ the classical δ-kicked rotor dynamics are globally chaotic, in the sense that there are no invariant tori that prevent trajectories in the main chaotic region from attaining arbitrarily large momenta. For K > 4 the primary resonances become unstable, and the phase space is predominantly chaotic.

The effects of a nonzero pulse width can be seen by rewriting the sequence of kicks as a discrete Fourier series and analyzing the amplitudes of the primary resonances of the system. Applying this procedure to the Hamiltonian (2),

$$H = \rho^2/2 + k \sum_{m=-\infty}^{\infty} \tilde{f}(2\pi m)\cos(\phi - 2\pi m\tau), \quad (3)$$

where $\tilde{f}(2\pi r)$ is the Fourier transform of the pulse function $f(\tau)$. This Hamiltonian has primary resonances located at $\rho = d\phi/dt = 2\pi m$. Therefore, the Fourier transform evaluated at $m = \rho/2\pi$ modifies the effective stochasticity parameter K_{eff} as a function of momentum. For a square pulse, which approximates the pulse used in our experiments, this factor can be written as

$$K_{eff} = \alpha k \frac{\sin(\alpha\rho/2)}{\alpha\rho/2}, \quad (4)$$

where $K_{eff}(\rho = 0) = \alpha k$ plays the role of the δ-kicked rotor stochasticity parameter K. This dependence of K_{eff} on momentum is displayed in Fig. 1, which compares several square-pulse cases to the δ-kick case. The dynamics of the system undergo a transition as K_{eff} drops to ~1, because of the presence of KAM surfaces that span the phase space and act as a barrier against momentum diffusion.

A simple classical model of the boundary provides us with relevant scaling parameters and makes clear the advantage of using cesium rather than sodium. Consider an atom with a momentum such that it travels one period of the standing wave during a kick. Then the momentum transferred to the atom by the potential averages to zero, and the particle no longer diffuses. This situation occurs when $vt_p = \lambda/2$, and hence an estimate for the boundary location is

$$\frac{p}{2\hbar k_L} = \frac{M\lambda^2}{8\pi\hbar t_p}. \quad (5)$$

Notice that this expression corresponds to the first zero-crossing of (4). The larger mass and longer optical wavelength of cesium provide a twelvefold increase over sodium in the momentum boundary location for a given pulse width.

3. EXPERIMENT

Our experimental setup (Fig. 2) is similar to that of our earlier sodium-based quantum chaos experiments [10]. The experiments are performed on laser-cooled cesium atoms in a magneto-optic trap (MOT) [14, 15].

The atoms are trapped in a stainless steel UHV chamber, in contrast to the earlier experiments in our group that used a quartz interaction chamber. All optical viewports are anti-reflection coated on both sides to reduce intensity fringes on the laser beams. An ampule containing cesium metal is attached to the chamber through a valve that is opened occasionally to leak cesium vapor into the chamber. The valve is necessary because of the rather high room temperature vapor pressure of cesium. A pair of anti-Helmholtz coils surrounding the chamber provides a magnetic field gradient of 11 G/cm for the MOT. When the current to the anti-Helmholtz coils is switched off, the magnetic fields decay exponentially after a brief transient, with a 1/e time of about 3 ms. This decay time is longer than in the earlier sodium-based experiments because of induced currents in the metal chamber.

Two single-mode diode lasers (L1, L2) at 852 nm provide the light for cooling, trapping, and detection of the cesium atoms. L1 is a 100 mW Distributed Bragg Reflector diode laser locked via frequency-modulation (FM) saturated-absorption spectroscopy to the $(6S_{1/2}, F = 4) \longrightarrow (6P_{3/2}, F' = 4, 5)$ crossover resonance. The main beam from L1 is double-passed through a tunable acousto-optic modulator (AOM1)
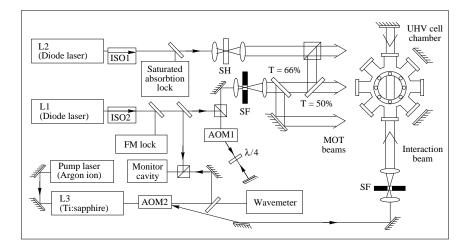
Fig. 2. Schematic diagram of the experimental setup. Two diode lasers provide the light for the MOT, and a Ti : sapphire laser provides the far-detuned standing wave.

centered at 80 MHz that provides fast control over the intensity and detuning of the beam. During the trapping stage of the experiment, the light from L1 is tuned 15 MHz to the red of the $(6S_{1/2}, F = 4) \longrightarrow (6P_{3/2}, F' = 5)$ cycling transition. The light from L1 passes through a spatial filter (SF), is collimated with a waist of 1.4 cm, and has a typical power of 23 mW at the chamber. The beam is divided into three beams of equal intensity by two beamsplitters with transmissions of 66 and 50%. The three beams are retroreflected through the center of the chamber in a standard six-beam MOT configuration.

The repump laser, L2, is a 150 mW Littrow-cavity, grating-stabilized diode laser. This beam is used to prevent optical pumping into the $F = 3$ ground state during the trapping and detection stages. This laser is electronically locked to the center of the $(6S_{1/2}, F = 3) \longrightarrow (6P_{3/2}, F' = 4)$ saturated absorption resonance. The beam has a typical power of 27 mW at the chamber and a waist of 7.5 mm. The intensity is controlled by a mechanical shutter (SH) with a rise/fall time of 1 ms. The beam is combined with the vertical arm of the light from L1 via a polarizing cube beamsplitter and retro-reflected through the chamber. Optical isolators (ISO1, ISO2) are used to minimize optical feedback to L1 and L2.

The entire experimental timing and data acquisition sequences are computer controlled. After trapping and initial cooling, the intensity of L1 is reduced for 1 ms and the detuning is increased to 39 MHz to further cool the sample. Typically, we trap 10^6 atoms from the background vapor. The momentum distribution of the atoms is nearly Gaussian, although the tails of the distribution are more populated than in a purely Gaussian distribution. The center of the distribution typically fits well to a Gaussian distribution with $\sigma_p/2\hbar k_L = 4.4$, and 96% of the atoms are contained in this Gaussian. The position distribution of the atoms is also Gaussian, with $\sigma_x = 0.1$ mm.

After the final cooling, the trapping fields are turned off, leaving the momentum distribution unchanged, and the interaction potential pulses are then turned on. A stabilized single-mode Ti : sapphire laser (L3) pumped by an argon-ion laser provides the pulsed standing wave. The light from L3 passes through a fixed-frequency 80 MHz acousto-optic modulator (AOM2) that controls the pulse sequence. The beam is spatially filtered, centered on the atoms, and retro-reflected through the chamber to form a standing wave. The beam has a typical power of 290 mW at the chamber and a waist of 1.44 mm. The absolute wavelength of L3 is measured with a scanning Michelson interferometer wavemeter. A scanning confocal Fabry–Perot cavity with a 1.5 GHz free spectral range is used to monitor long-term drift of L3 during measurements.

For all the experiments described here we detuned this beam 6.1 GHz to the red of the cycling transition, with typical fluctuations of about 100 MHz. The pulse sequence consisted of a series of fixed-length pulses with a rise/fall time of 75 ns and less than 3 ns variation in the pulse duration. Sequences using pulse widths between 283 and 1975 ns (full width at half maximum) were used in these experiments to demonstrate the role of the momentum boundary. The period was 20 μs with less than 4 ns variation per pulse period as measured with a fast photodiode. The probability of spontaneous scattering was less than 0.5% per kick period for all of the parameters used. The phase noise of the standing wave due to vibrations in the optical system resulted in less than 8% of a standing wave period phase drift after 200 kicks, with a typical fluctuation timescale of 0.5 ms.

The detection of momentum is accomplished by a time-of-flight method. The atoms drift in the dark for a controlled duration, typically 15 ms. The trapping
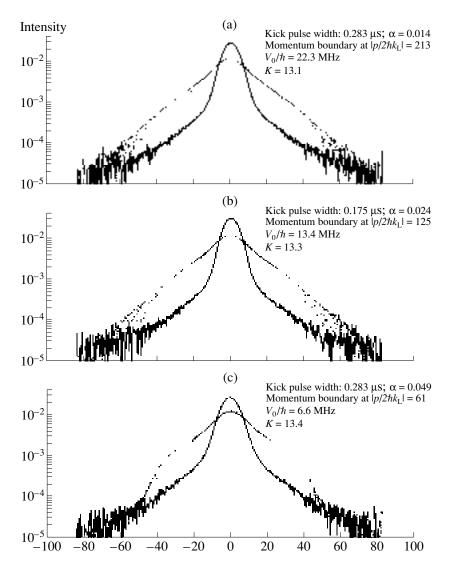
Intensity

(a)

Kick pulse width: 0.283 μs; $\alpha = 0.014$
Momentum boundary at $|p/2\hbar k_L| = 213$
$V_0/\hbar = 22.3$ MHz
$K = 13.1$

10^{-2}

10^{-3}

10^{-4}

10^{-5}

(b)

Kick pulse width: 0.175 μs; $\alpha = 0.024$
Momentum boundary at $|p/2\hbar k_L| = 125$
$V_0/\hbar = 13.4$ MHz
$K = 13.3$

10^{-2}

10^{-3}

10^{-4}

10^{-5}

(c)

Kick pulse width: 0.283 μs; $\alpha = 0.049$
Momentum boundary at $|p/2\hbar k_L| = 61$
$V_0/\hbar = 6.6$ MHz
$K = 13.4$

10^{-2}

10^{-3}

10^{-4}

10^{-5}
  -100 -80 -60 -40 -20 0   20   40   60   80   100$

Fig. 3. Comparison of momentum distribution evolution for 4 different kick pulsewidths from 0.3 to 2μs. Distributions for 5 different times are shown on each graph: 0 kicks (heavy solid line), 17 kicks (dotted), 34 kicks (dashed), 51 kicks (dash–dot), and 62 kicks (solid). This data shows the effect of the boundary on the evolution of the momentum distribution. The vertical scales are logarithmic and in arbitrary units.

beams are then turned on in zero magnetic field, forming an optical molasses [14] that freezes the position of the atoms. The final spatial distribution is recorded via fluorescence imaging in a short (10 ms) exposure on a cooled charge-coupled device (CCD) camera. The final distribution and the free-drift time enable the determination of the momentum distribution. The maximum momentum that we can measure is limited by the size of the CCD. For a 15 ms drift time, we can detect momenta within $|p/2\hbar_L| \approx 80$. Using shorter drift times, we could measure larger momenta at the expense of resolution. The initial spatial distribution is not deconvolved from the final momentum distributions, because the effect on the RMS width of our final distributions is on the order of one percent.

The pulse period was $T = 20$ μs, corresponding to $\bar{k} = 2.08$. The kick strength k was chosen to provide the best exponentially localized momentum distributions. For the shortest pulses, we used $V_0/h = 3.55$ MHz, yielding a classical stochasticity parameter of $K = 13.1$. For the longest pulses we used $V_0/h = 0.94$ MHz, corresponding to $K = 24$. The absolute uncertainty in K is $\pm 10\%$, and the largest contributions are due to the measurement of beam profile and the absolute laser power calibration.

The momentum boundary due to the nonzero pulse width is $|p/2\hbar k_L| = 213$ for our typical operating parameters. This value is a factor of four larger than in our earlier sodium experiments. The corresponding reduction in the effective value of K is only 6% out to

$|p/2\hbar k_L| = 40$ and 25% at our maximum detectable momentum of $|p/2\hbar k_L| \approx 80$.

Figure 3 presents experimental data using three different pulse widths in order to study the effects of momentum boundaries as predicted by (5). In each case, the distributions are taken at increments of 17 kicks. In the first case, Fig. 3a, the boundary of $|p/2\hbar k_L| = 213$ is three times larger than the $|p/2\hbar k_L| = 70$ resolvable width of our distribution. This situation is ideal for experimental studies of the quantum kicked rotor, since the momentum distribution remains well within the boundary. In Fig. 3b, we see that although the distance between the boundaries at $|p/2\hbar k_L| = 125$ is less than twice the width of the final distribution, there is little effect on the shapes of the distributions. In Fig. 3c, the boundary is located at $|p/2\hbar k_L| = 61$, and it has a clear effect on the wings of the distributions. Notice, however, that after 17 kicks the distribution still looks exponential.

The dynamics near the center of the distribution appear to be relatively insensitive to the location of the boundary. Nevertheless, the energy of the distribution can be strongly affected by the boundary, and is therefore less important than the momentum distributions themselves. This point is significant because much of the theoretical analysis of this system has been done using the long-term diffusion in energy, which is especially sensitive to the high-momentum tails of the distribution.

4. SUMMARY AND FUTURE DIRECTIONS

We have constructed a new quantum chaos experiment in cesium that is capable of a much wider range of experiments than the first generation sodium-based experiments. The primary advantage of this new experiment lies in the physical characteristics of cesium, which reduce the effects of the momentum boundary and bring the experiment closer to the δ-kick limit. We are now studying the effects of noise and decoherence on localization and have obtained first experimental results. We are also studying the effects of classical structures in phase space on quantum transport.

REFERENCES

1. Casati, G., Chirikov, B.V., Ford, J., and Izrailev, F.M., 1979, *Stochastic Behaviour in Classical and Quantum Hamiltonian Systems*, vol. 93, of *Lecture Notes in Physics*, Casati, G. and Ford, J., Eds. (Berlin: Springer).
2. Chirikov, B., Izrailev, F.M., and Shepelyansky, D.L., 1981, *Sov. Sci. Rev. C*, **2**, 209.
3. Fishman, S., Grempel, D.R., and Prange, R.E., 1982, *Phys. Rev. Lett.*, **49**, 509; Grempel, D.R., Prange, R.E., and Fishman, S., 1984, *Phys. Rev. A*, **29**, 1639.
4. Shepelyansky, D.L., 1982, *Physica D*, **8**, 208.
5. Shepelyansky, D.L., 1986, *Phys. Rev. Lett.*, **56**, 677; Shepelyansky, D.L., 1987, *Physica D*, **28**, 103.
6. Cohen, D., 1991, *Phys. Rev. A*, **44**, 2292.
7. Blumel, R. and Reinhardt, W.P., 1997, *Chaos in Atomic Physics* (Cambridge).
8. Moore, F.L., Robinson, J.C., Bharucha, C.F., *et al.*, 1994, *Phys. Rev. Lett.*, **73**, 2974.
9. Robinson, J.C., Bharucha, C.F., Moore, F.L., *et al.*, 1995, *Phys. Rev. Lett.*, **74**, 3963.
10. Moore, F.L., Robinson, J.C., Bharucha, C.F., *et al.*, 1995, *Phys. Rev. Lett.*, **75**, 4598.
11. Robinson, J.C., Bharucha, C.F., Madison, K.W., *et al.*, 1996, *Phys. Rev. Lett.*, **76**, 3304.
12. Collins, G.P., 1995, *Phys. Today*, **48**, 18.
13. Graham, R., Schlautmann, M., and Zoller, P., 1992, *Phys. Rev. A*, **45**, R19.
14. Chu, S., 1991, *Science*, **253**, 861.
15. Cohen-Tannoudji, C., 1992, *Fundamental Systems in Quantum Optics, Les Houches*, 1990, Dalibard, J., Raimond, J.M., and Zinn-Justin, J., Eds. (London: Elsevier).